Editors' Suggestion

Quantization of fractional corner charge in C_n-symmetric higher-order topological crystalline insulators

Wladimir A. Benalcazar,[1,2,*] Tianhe Li,[2] and Taylor L. Hughes[2]

[1]*Department of Physics, The Pennsylvania State University, University Park, Pennsylvania 16802, USA*

[2]*Department of Physics and Institute for Condensed Matter Theory, University of Illinois at Urbana-Champaign, Illinois 61801, USA*

(Received 30 October 2018; revised manuscript received 6 June 2019; published 26 June 2019)

In the presence of crystalline symmetries, certain topological insulators present a *filling anomaly*: a mismatch between the number of electrons in an energy band and the number of electrons required for charge neutrality. In this paper, we show that a filling anomaly can arise when corners are introduced in C_n-symmetric crystalline insulators with vanishing polarization, having as a consequence the existence of corner-localized charges quantized in multiples of $\frac{e}{n}$. We characterize the existence of this charge systematically and build topological indices that relate the symmetry representations of the occupied energy bands of a crystal to the quanta of fractional charge robustly localized at its corners. When an additional chiral symmetry is present, $\frac{e}{2}$ corner charges are accompanied by zero-energy corner-localized states. We show the application of our indices in a number of atomic and fragile topological insulators and discuss the role of fractional charges bound to disclinations as bulk probes for these crystalline phases.

DOI: 10.1103/PhysRevB.99.245151

Topological crystalline insulators (TCIs) [1–7] are known to exhibit a variety of quantized electromagnetic phenomena. They host bulk dipole moments that lead to surface charge densities quantized in fractions of the electronic charge e [8–13]. Recently, it was found that TCIs can also host higher bulk multipole moments that manifest lower-order moments bound to their boundaries [14,15]. For example, a quadrupole insulator in two dimensions has edge-bound dipole moments and corner-bound charges, while an octupole insulator in three dimensions has surface-bound quadrupole moments, hinge-bound dipole moments, and corner-bound charges. Just as in the case of insulators with symmetry-protected dipole moments, crystalline symmetries quantize the boundary signatures in quadrupole or octupole TCIs. Indeed, TCIs with quantized multipole moments are symmetry protected topological phases of matter; their quantization is robust and can change only in discrete jumps at phase transitions [14,15], unless the protecting symmetries are broken.

A salient property of TCIs with quantized higher multipole moments is that some of their protected observables at the boundary are at least two dimensions less than the protecting bulk. This property has now been extended to a broader family of TCIs, broadly referred to as higher-order topological insulators [15–41]. In this paper, we focus on two-dimensional (2D) higher-order TCIs having zero-dimensional topological signatures. A number of studies have recently shown examples of such TCIs which exhibit in-gap corner-localized states [15,21–27], some of which have been related to fractionally quantized corner charges [15,22,23,27]. Interestingly, many such TCIs have these corner signatures in spite of vanishing quadrupole moments, and their mechanisms of protection and associated topological invariants are still not completely elucidated.

In this paper we systematically study 2D second-order TCIs in class AI (spinless and time-reversal symmetric insulators) protected by C_n symmetry and find the topological indices that connect the bulk topology of these TCIs with corner or defect-bound fractional charges. We show that the fractional quantization of corner charge arises from a *filling anomaly*: a topological property of the occupied energy bands of a TCI that keeps track of the mismatch between the number of electrons required to simultaneously satisfy charge neutrality and the crystal symmetry. This mismatch exists even in first-order TCIs with quantized dipole moments—giving rise to quantized fractional charge at edges [10,12,42–44]—and we discuss this type of filling anomaly to introduce the concept. Our focus, however, is on a refined form of a filling anomaly that originates *only* when corners are created in a lattice. Such corner-induced filling anomalies are particular of higher-order topological phases. We build topological indices that allow us to identify the cases in which the filling anomaly arising from edges is avoided, but the filling anomaly due to corners is not. Given the set of rotation topological invariants for a particular C_n symmetry (extracted from the representations of the little groups of the occupied bands at the high symmetry points of the Brillouin zone), the topological indices we derive relate the set of rotation topological invariants to the quanta of the corner-bound charge. We show that in obstructed atomic insulators, i.e., insulators that admit a Wannier representation [45], the filling anomaly is intimately related to the locations of the Wannier centers of the electrons in the bulk of the crystal. However, the index theorems apply even for crystalline insulators that are *not* Wannier representable, as we will show by providing examples for the quantization

*wladimir.benalcazar@psu.edu

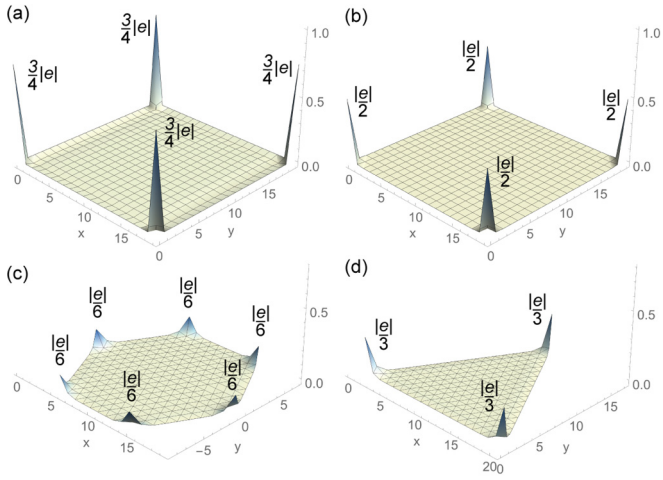

FIG. 1. Quantized fractional corner charge in C_n-symmetric TCIs. The plots show the total (electronic and ionic) charge density of two-dimensional TCIs. (a) a C_4-symmetric TCI with corner charge $\frac{3|e|}{4}$, (b) a C_4-symmetric TCI with corner charge $\frac{|e|}{2}$, (c) a C_6-symmetric TCI with corner charge $\frac{|e|}{6}$, and (d) a C_3-symmetric TCI with corner charge $\frac{|e|}{3}$. In all cases, the bulk *and* edges are neutral. These charge patterns are obtained by stacking the primitive generator models as described in Sec. V.

of charge fractionalization at the corners of fragile topological crystalline phases [46–49].

The paper is organized as follows. In Sec. I, we first classify C_n-symmetric TCIs in terms of rotation topological invariants which we define (see Refs. [23,50–53] for other related invariants and classifications). In Sec. II, we present model Hamiltonians that constitute *primitive generators* of these classifications. All of our generators are Wannier representable [45,54–57] and have the property that they can be combined to span the entire set of phases in these classifications. The Wannier representability of our generators is advantageous because it transparently connects the Wannier centers of the electrons in the bulk and boundaries of a lattice to the filling anomaly and consequently to the edge and corner charge. Additionally, because of their simple structure and our choice of the AI symmetry class, all of our generator models can be straightforwardly constructed in metamaterial contexts through the evanescent coupling of waveguide or resonator modes. This will allow for the immediate realization of our predictions in experiments.

After introducing the generators, in Secs. III and IV we describe the mechanism that gives rise to the edge and corner filling anomalies, respectively, and how they relate to edge and corner fractional charges. In Sec. V we apply our insights from the previous sections to identify the boundary charges in the primitive generators, which we then use to build index theorems for the filling anomaly and corner fractional charge of any C_n-symmetric higher-order TCI in class AI. We find that TCIs in a lattice with a global C_n-symmetry host corner-localized charges that, when added within a spatial sector subtended by an angle of $\frac{2\pi}{n}$ from the center of the lattice, are quantized in multiples of $\frac{e}{n}$. In particular, if each $\frac{2\pi}{n}$ sector has only one corner, the charge is fractionally quantized at each corner of the lattice, as shown in Fig. 1.

After the construction of the topological indices, in Sec. VI we provide examples of the fractional quantization of charge in TCIs without a Wannier representation, and in Sec. VII we apply our theory to show that higher-order TCIs bind fractional charge at the core of certain topological defects. Finally, we present a discussion and our conclusions in Sec. VIII.

I. CLASSIFICATION

Two-dimensional TCIs in class AI [58–60] preserve time-reversal symmetry (TRS), having Bloch Hamiltonians satisfying $h(\mathbf{k}) = h^*(-\mathbf{k})$. These systems have a vanishing Hall conductance, indicated by a zero Chern number. The presence of additional C_n symmetry, however, allows for a finer classification of topological phases in these insulators [2,23,50–53] (see Appendix A in Ref. [61] for the detailed construction of the classification). These classes can be most directly distinguished by the value of their polarization [8–11,62–64]

$$\mathbf{P}^{(n)} = p_1\mathbf{a_1} + p_2\mathbf{a_2}, \tag{1}$$

where the superindex n labels the C_n symmetry of the classification, $\mathbf{a_1}$ and $\mathbf{a_2}$ are primitive unit lattice vectors, and the components p_1 and p_2 are topological indices that correspond to quantized Berry phases along the noncontractible loops of the Brillouin zone (BZ) [8,12,13,50]. We take $\mathbf{a_1}$ and $\mathbf{a_2}$ to be $\mathbf{a_1} = \hat{\mathbf{x}}$, $\mathbf{a_2} = \hat{\mathbf{y}}$ in C_4 and C_2-symmetric lattices, and $\mathbf{a_1} = \hat{\mathbf{x}}$, $\mathbf{a_2} = \frac{1}{2}\hat{\mathbf{x}} + \frac{\sqrt{3}}{2}\hat{\mathbf{y}}$ in C_6 and C_3-symmetric lattices (note that we have set all lattice constants to unity). As reviewed in Appendix B in Ref. [61], the values of the polarization $\mathbf{P}$ form a $\mathbb{Z}_2$ index in C_4-symmetric TCIs as it can only take the values $p_1 = p_2 \in \{0, \frac{e}{2}\}$, a $\mathbb{Z}_2 \times \mathbb{Z}_2$ index in C_2-symmetric TCIs with values $p_1, p_2 \in \{0, \frac{e}{2}\}$, and a $\mathbb{Z}_3$ index in C_3-symmetric TCIs with values $p_1 = p_2 \in \{0, \frac{e}{3}, \frac{2e}{3}\}$; while in C_6-symmetric TCIs the polarization always vanishes.

More generically, we can distinguish nontrivial topological classes arising from the C_n symmetry through the symmetry representations that the occupied energy bands take at the high symmetry points of the BZ (HSPs) [2,45,50,52,53,65,66]. Consider C_n-symmetric Bloch Hamiltonians, which obey $\hat{r}_n h(\mathbf{k})\hat{r}_n^\dagger = h(R_n\mathbf{k})$, where $\hat{r}_n$ is the n-fold rotation operator obeying $\hat{r}_n^n = 1$, and R_n is the n-fold rotation matrix acting on the crystal momentum $\mathbf{k}$. We denote the HSPs as $\mathbf{\Pi}^{(n)}$. These are defined as the special points in the BZ which obey $R_n\mathbf{\Pi}^{(n)} = \mathbf{\Pi}^{(n)}$ modulo a reciprocal lattice vector. Rotation symmetry then implies that $[\hat{r}_n, h(\mathbf{\Pi}^{(n)})] = 0$. Thus, the energy eigenstates of the Bloch Hamiltonian at HSPs are also eigenstates of the rotation operator. Let us denote the eigenvalues of $\hat{r}_n$ at HSP $\mathbf{\Pi}^{(n)}$ as

$$\Pi_p^{(n)} = e^{2\pi i(p-1)/n}, \quad \text{for } p = 1, 2, \ldots n, \tag{2}$$

(see a complete list of HSPs in Appendix A in Ref. [61]). Given a subspace of energy bands, we can compare these rotation eigenvalues at the various HSPs. If the eigenvalues change at different HSPs, the energy bands have nontrivial topology. Accordingly, we use the rotation eigenvalues at $\mathbf{\Pi}^{(n)}$ compared to a reference point $\mathbf{\Gamma} = (0, 0)$ to define the integer topological invariants

$$\left[\Pi_p^{(n)}\right] \equiv \#\Pi_p^{(n)} - \#\Gamma_p^{(n)}, \tag{3}$$

where $\#\Pi_p^{(n)}$ is the number of energy bands below the (in-gap) Fermi level with eigenvalue $\Pi_p^{(n)}$. Not all these invariants are independent, however. First, rotation symmetry can force representations at certain HSPs to be the same. C_4 symmetry forces the representations at $\mathbf{X}$ and $\mathbf{X}'$ in the BZ to be equal, while C_6 symmetry forces equal representations at $\mathbf{M}$, $\mathbf{M}'$, and $\mathbf{M}''$, as well as at $\mathbf{K}$ and $\mathbf{K}'$. Furthermore, there are redundancies in the invariants due to: (i) the fact that the number of bands in consideration is constant across the BZ, from which it follows that $\sum_p \#\Pi_p^{(n)} = \sum_p \#\Gamma_p^{(n)}$, or $\sum_p [\Pi_p^{(n)}] = 0$, and (ii) the existence of TRS, which implies that rotation eigenvalues at $\mathbf{\Pi}^{(n)}$ and $-\mathbf{\Pi}^{(n)}$ are related by complex conjugation, from which it follows that $[M_2^{(4)}] = [M_4^{(4)}]$, $[K_2^{(3)}] = [K_3^{'(3)}]$, and $[K_3^{(3)}] = [K_2^{'(3)}]$. Dropping the redundant invariants due to these constraints, the resulting topological classes of TCIs with TRS and C_n symmetry are given by the indices $\chi^{(n)}$, as follows,

$$\begin{aligned}
\chi^{(4)} &= \left([X_1^{(2)}], [M_1^{(4)}], [M_2^{(4)}]\right)\\
\chi^{(2)} &= \left([X_1^{(2)}], [Y_1^{(2)}], [M_1^{(2)}]\right)\\
\chi^{(6)} &= \left([M_1^{(2)}], [K_1^{(3)}]\right)\\
\chi^{(3)} &= \left([K_1^{(3)}], [K_2^{(3)}]\right).
\end{aligned} \tag{4}$$

The C_2 invariants of a C_4-symmetric insulator obey $[X_1^{(2)}] = [Y_1^{(2)}]$ and $[M_1^{(2)}] = -2[M_2^{(4)}]$, and the C_3 invariants of a C_6-symmetric insulator obey $[K_1^{(3)}] = [K_2^{(3)}]$. C_n-symmetric TCIs with different $\chi^{(n)}$ belong to different topological classes, as they cannot be deformed into one another without closing the bulk energy gap or breaking the symmetry [52,53,60,67]. Not all possible values of $\chi^{(n)}$ correspond to insulating phases; some points in these classification spaces are forced to be gapless by symmetry (e.g., when in $\chi^{(2)}$ we have $[X_1^{(2)}] + [Y_1^{(2)}] + [M_1^{(2)}] = 1$ mod 2 the crystal is gapless) [66]. Nevertheless, all C_n symmetric TCIs do have a corresponding point in its $\chi^{(n)}$ classification space.

Having identified the rotation invariants that distinguish the C_n protected topological phases, we can apply the algebraic method developed in Refs. [52,53] to connect these invariants to physical properties. The topological classification $\chi^{(n)}$ forms a free Abelian additive structure. Two C_n-symmetric TCIs with Hamiltonians $h_1^{(n)}$ and $h_2^{(n)}$, in classes $\chi_1^{(n)}$ and $\chi_2^{(n)}$, and having rotation operators $\hat{r}_n$ and $\hat{r}'_n$, respectively, can be stacked leading to a third C_n-symmetric insulator with Hamiltonian $h_3^{(n)} = h_1^{(n)} \oplus h_2^{(n)}$ and with rotation operator $\hat{r}''_n = \hat{r}_n \oplus \hat{r}'_n$. The resulting insulator is in class $\chi_3^{(n)} = \chi_1^{(n)} + \chi_2^{(n)}$. Thus, given a C_n symmetry which classifies TCIs using N topological invariants, all topological classes—and their topological observables—can be accessed by a set of N *primitive generators*: a set of C_n-symmetric TCIs having invariants represented by vectors $\chi^{(n)}$ which are linearly independent to one another. From the classifications in Eq. (4), it follows that all of our topological classes can be accessed by combinations of three primitive generators for each of C_4 and C_2-symmetric TCIs, and by two primitive generators for each of C_6 and C_3-symmetric TCIs.

II. PRIMITIVE GENERATORS

The primitive generators we consider are illustrated in Figs. 2(c)–2(f) and 3(c)–3(f). The shaded squares and hexagons delimit the unit cells. Within each unit cell, the black dots represent its degrees of freedom; for example, they could represent different ions—each hosting an electronic orbital—or different orbitals generated by a single ion [45]. Although the ionic charges do not enter the tight-binding Hamiltonians represented in this lattice, our formulation requires that each unit cell contains an integer ionic charge. In all our models, we assume the center of all the positive ionic charge is localized at the maximal Wyckoff position a of the unit cell (see Appendix C in Ref. [61] for a description of ionic positions and choices of unit cells) [black dots in Figs. 2(a), 2(b), 3(a), and 3(b)]. All the generators are TCIs that admit a Wannier representation [68,69] of their occupied bands.

The $\chi^{(n)}$ invariants of these generators are indicated in Table I. In the bulk, they are Wannier representable [68,69], with Wannier centers pinned, by symmetry, to maximal Wyckoff positions other than at the center of the unit cell. In contrast, trivial bands, in class $\chi^{(n)} = \mathbf{0}$, will necessarily have Wannier centers at the center of the unit cell, coinciding with the position of the ionic centers. Our primitive generators are in *obstructed atomic limits* [45,57], because a connection to the *trivial atomic limit* $\chi^{(n)} = \mathbf{0}$ is not allowed unless a gap-closing phase transition occurs or the symmetry is broken.

We present the generators in Figs. 2 and 3 in a simple limit without hopping terms within unit cells to allow a pictorial identification of the Wannier centers. Their topological classes are stable to the addition of intracell hopping terms or any other symmetry-preserving terms that do not close the bulk gap. In Appendix D in [61], we detail how adding intracell hopping terms can transition our models into a variety of classes in their $\chi^{(n)}$ classifications. Since our generators are spinless and only require real-valued hoppings (i.e., without any phase factors), they are easy to fabricate in a variety of metamaterials. Indeed, the lattices presented in Refs. [21,24] and [26] coincide with the generators shown in Figs. 2(c), 3(d), and 3(f), respectively. A first instance of a possible solid state material realization of one of these primitive generators is detailed in Ref. [22] for the generator shown in Fig. 3(f).

We use the notation that a generator $h_{mW}^{(n)}$ is C_n symmetric, has m filled bands, and has Wannier centers at the maximal Wyckoff positions W shown in Figs. 2(a), 2(b), 3(a), and 3(b). The classification of C_4-symmetric TCIs has three generators: $h_{1b}^{(4)}$, $h_{2b}^{(4)}$, and $h_{2c}^{(4)}$ [Figs. 2(c), 2(d), and 2(e)]. All of them have four energy bands. The lattice model in Fig. 2(c) has a gap that separates the first and the second bands, and another gap that separates the third and fourth bands. We take the first generator $h_{1b}^{(4)}$ to occupy only the lowest band, i.e., $\frac{1}{4}$ filling. The generators $h_{2b}^{(4)}$ and $h_{2c}^{(4)}$ are gapped at half filling; hence, we take both of these generators to occupy the lowest two bands. As indicated by their labels, the first two generators have one and two Wannier centers at position b, respectively [red dot in Fig. 2(a)], while the third generator has Wannier centers at the two inequivalent positions c and c' [blue dots in Fig. 2(a)].

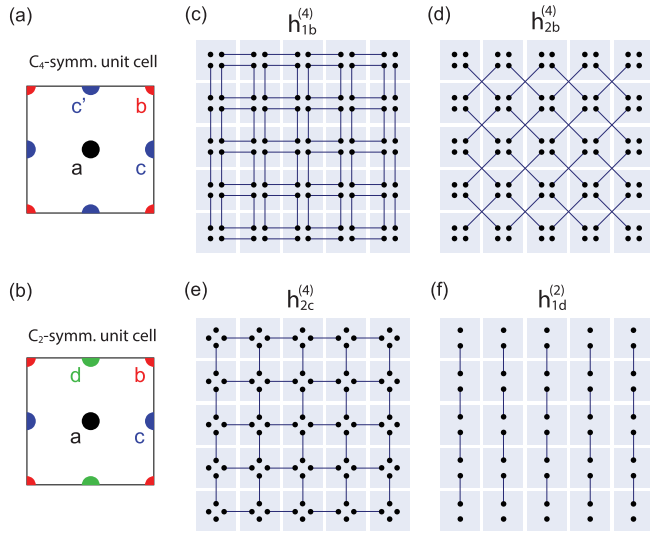

FIG. 2. (a), (b) Maximal Wyckoff positions for (a) C_4- and (b) C_2-symmetric unit cells. (c)–(e) Lattices for the three primitive generators that span the classification of C_4-symmetric TCIs. The lattices for the primitive generators for the classification of C_2-symmetric TCIs are those in (c), (e), and (f).

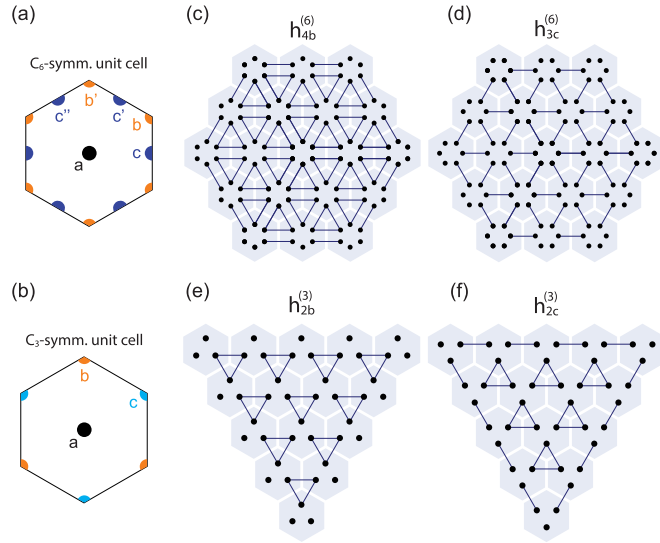

FIG. 3. (a), (b) Maximal Wyckoff positions for (a) C_6- and (b) C_3-symmetric unit cells. (c), (d) Primitive generators that span the classification of C_6-symmetric TCIs. (e), (f) Primitive generators for the classification of C_3-symmetric TCIs.

The classification of C_2-symmetric TCIs also requires three generators. We choose the first two of them to be $h^{(4)}_{1b}$ and $h^{(4)}_{2c}$ [Figs. 2(c) and 2(e)]. The generator $h^{(4)}_{2b}$ is not independent because its C_2 invariants are given by the vector $\chi^{(2)} = (2, 2, 0)$, which is linearly proportional to the invariant vector of $h^{(4)}_{1b}$, $\chi^{(2)} = (-1, -1, 0)$. The third generator is a two-dimensional version of the Su-Schrieffer-Heeger (SSH) model [70], labeled as $h^{(2)}_{1d}$ and shown in Fig. 2(f) in its extremely dimerized limit. As the label indicates, it is an obstructed atomic limit with one Wannier center at position d.

The classification of C_6-symmetric TCIs requires two generators. We take them to be $h^{(6)}_{4b}$ and $h^{(6)}_{3c}$ [Figs. 3(c) and 3(d)]. Both of them have six energy bands. $h^{(6)}_{4b}$ is taken to occupy the lowest four bands and has a pair of Wannier centers at each of the Wyckoff positions b and b' [orange dots in Fig. 3(a)], while $h^{(6)}_{3c}$ is taken to occupy the lowest three bands, and has its three Wannier centers at positions c, c', and c'' [blue dots in Fig. 3(a)].

The classification of C_3-symmetric TCIs requires two generators. We take them to be $h^{(3)}_{2b}$ and $h^{(3)}_{2c}$ [Figs. 3(e) and 3(f)], which are related to each other by a π rotation. Each of these generators has three energy bands with a degeneracy in the lowest two bands protected by C_3 symmetry and TRS at the $\mathbf{\Gamma}$ point. We therefore take these two models to occupy the lowest two energy bands. $h^{(3)}_{2b}$ has its two Wannier centers at the Wyckoff position b [orange dot in Fig. 3(b)], while $h^{(3)}_{2c}$ has them at position c [cyan dot in Fig. 3(b)]. In Appendix E in Ref. [61] we induce the representations for Wannier orbitals at all maximal Wyckoff positions for all the C_n-symmetric configurations, and by comparing these representations with those of our primitive generators, show that they have the Wannier centers described in this section.

III. FILLING ANOMALY AND CHARGE FRACTIONALIZATION: POLARIZATION

Due to the crystalline symmetry of a TCI, it may be impossible to maintain the number of electrons required for charge neutrality. To illustrate the simplest case in which this happens, consider the SSH model [70], which has the Bloch Hamiltonian

$$h^{SSH}(k) = \begin{pmatrix} 0 & t_0 + t_1 e^{ik} \\ t_0 + t_1 e^{-ik} & 0 \end{pmatrix}. \tag{5}$$

This model has a reflection symmetry,

$$\hat{M} h^{SSH}(k) \hat{M}^{-1} = h^{SSH}(-k), \quad \hat{M} = \begin{pmatrix} 0 & 1 \\ 1 & 0 \end{pmatrix},$$

that protects two gapped phases separated by a gapless point at $t_0 = t_1$. We consider this insulator with electrons occupying only the lowest energy band. At this filling, and with periodic boundary conditions, each unit cell has only one electron. To have a neutral insulator, each unit cell in the crystal has one positive ion with charge $|e|$. When we open the boundaries (with edge terminations that do not cut inside unit cells), on the other hand, the number of electrons is different at each phase. When $t_0 > t_1$, $h^{SSH}(k)$ is in the trivial atomic limit and its Wannier centers are as shown in Fig. 4(a). In the other phase, $t_0 < t_1$, $h^{SSH}(k)$ is in an obstructed atomic limit with Wannier centers as shown in Fig. 4(b). Notice that in the trivial phase there is charge neutrality: For N ions in the crystal (one per unit cell), there are N electrons and the configuration is reflection symmetric. On the other hand, in the obstructed atomic limit, charge neutrality is lost: For N ions, there are either $N - 1$ or $N + 1$ electrons. Reflection symmetry in $h^{SSH}(k)$ guarantees pairwise degeneracies in the energies of the electronic states at the boundaries. Thus, raising the Fermi level can transition from $N - 1$ to $N + 1$ electrons but not from $N - 1$ to N which would be needed for neutrality.

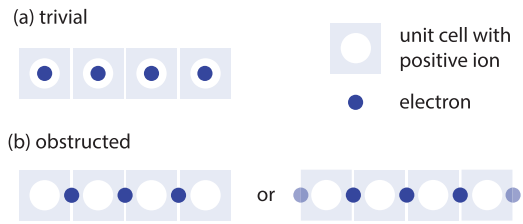

FIG. 4. Filling anomaly in the reflection symmetric Su-Schrieffer-Hegger model with the Bloch Hamiltonian of Eq. (5) and open boundaries. (a) Trivial atomic limit. Charges are balanced. (b) Obstructed atomic limit. Positive and negative charges are unbalanced. For N positive ions, there are $N-1$ electrons (left) or $N+1$ electrons (right). Solid (dimmer) circles represent bulk (boundary) Wannier centers.

More generically, for a preserved crystalline symmetry that divides a lattice into n symmetry-related sectors, we can define a *filling anomaly* to be

$$\eta = \#\text{ions} - \#\text{electrons} \mod n. \tag{6}$$

Thus, in the case of reflection symmetry, which divides the lattice into left and right halves, the filling anomaly (defined modulo 2) captures the parity of charge imbalance. Reflection symmetry guarantees that any extra charge due to charge imbalance in the obstructed atomic limit is distributed equally among the two halves of the lattice. Thus, when the charge imbalance is odd we will have fractional charge $\frac{e}{2}$ modulo $|e|$ in each sector. This happens for the obstructed atomic limit, which has a dipole moment of $p = \frac{e}{2}$; hence, the filling anomaly due to edges is a manifestation of the bulk-boundary correspondence for polarization.

We now extend the formulation of the filling anomaly to TCIs with dipole moments in two dimensions. Let us consider vertically aligned SSH chains having N_y unit cells along y. We stack N_x such chains along the x direction as in $h^{(2)}_{1d}$ [Fig. 2(f)] to form a two-dimensional lattice with open boundaries along y. To avoid introducing corners, we impose periodic boundary conditions along x. The charge imbalance in the obstructed atomic limit will be N_x. Following the analysis for the one-dimensional case, we can define the charge density at each of the (upper or lower) halves of the lattice *per unit cell along x* by

$$\rho = \frac{\#\text{ions} - \#\text{electrons}}{2N_x}|e| \mod |e|, \tag{7}$$

where the denominator has a factor of 2 due to the two symmetry-related halves and a factor of N_x to determine the charge per unit length. The charge density in Eq. (7) captures the usual fractionalization of edge charge density due to a bulk polarization that is quantized under symmetries [8,10,12,13]. It is useful to note that the filling mismatch associated with polarization scales with the system size along x, N_x. The definition of charge density in Eq. (7) also provides us with a microscopic picture of charge fractionalization; in the extremely dimerized limits we are considering, the fractional boundary charge can be pictorially determined by counting the fraction of bulk Wannier orbitals that fall into the boundary unit cells modulo $|e|$ [e.g., only half of a bulk Wannier orbital falls into the boundary unit cell in Fig. 4(b), right].

In previous work, the polarization components $p_{i=1,2}$ [Eq. (1)] of reflection or inversion symmetric TCIs were related to the inversion or reflection symmetry eigenvalues that the occupied states take at the HSPs [12,13]. Extending this approach to C_n symmetries [50], the values of polarization in terms of the invariants of Eq. (4) (detailed in Appendix B in Ref. [61]) are

$$\begin{aligned}
\mathbf{P}^{(4)} &= \frac{e}{2}\big[X_1^{(2)}\big](\mathbf{a_1}+\mathbf{a_2}) \\
\mathbf{P}^{(2)} &= \frac{e}{2}\big(\big[Y_1^{(2)}\big]+\big[M_1^{(2)}\big]\big)\mathbf{a_1} + \frac{e}{2}\big(\big[X_1^{(2)}\big]+\big[M_1^{(2)}\big]\big)\mathbf{a_2} \\
\mathbf{P}^{(6)} &= \mathbf{0} \\
\mathbf{P}^{(3)} &= \frac{2e}{3}\big(\big[K_1^{(3)}\big]+2\big[K_2^{(3)}\big]\big)(\mathbf{a_1}+\mathbf{a_2}),
\end{aligned} \tag{8}$$

all of which are defined modulo e. These indices can be directly applied to our primitive generators to determine their polarizations. Furthermore, the surface charge theorem immediately relates the bulk polarization to a surface charge density and, for our C_n protected TCIs, yields a quantized fractional charge per edge unit cell. The values of polarization for our primitive generators are indicated in Table I.

IV. FILLING ANOMALY AND CHARGE FRACTIONALIZATION: CORNER CHARGE

When a TCI has two open edges that intersect to form a corner, a filling anomaly arising from the corner itself may occur. This filling anomaly lies at the heart of higher-order topological insulators in two dimensions. In the initial study of topological quadrupole insulators, for example, there was a recognition that an overall charge imbalance exits in the subspace of occupied bands [14,15], which has later been found in other higher-order topological phases [27,40,41]. The work by Song *et al.* [17] additionally identified that, in higher-order TCIs that allow a Wannier representation, a mismatch exists between the Wannier centers of the occupied bands and the atomic positions in the crystal. Here, we connect the notion of Wannier center mismatch with the overall deficit of charge in energy bands by considering the bulk and edge electrons in real space representations of higher-order topological bands. This will allow us to put forward a formal definition of the filling anomaly in two dimensions and to relate all the possible filling anomalies to topological indices [Eq. (11)] written in terms of the topological invariants defined in Eq. (4).

For this purpose, we will use of our primitive generators defined in Sec. II. The connection between real space and crystal momentum space via our Wannier-representable primitive generators will make evident the connection between this higher-order filling anomaly and the quantization of fractional corner charge. Our topological indices, however, are more general than the primitive generators they are derived from, and are valid also for TCIs that are not Wannier representable, as we will show for fragile phases in Sec. VI.

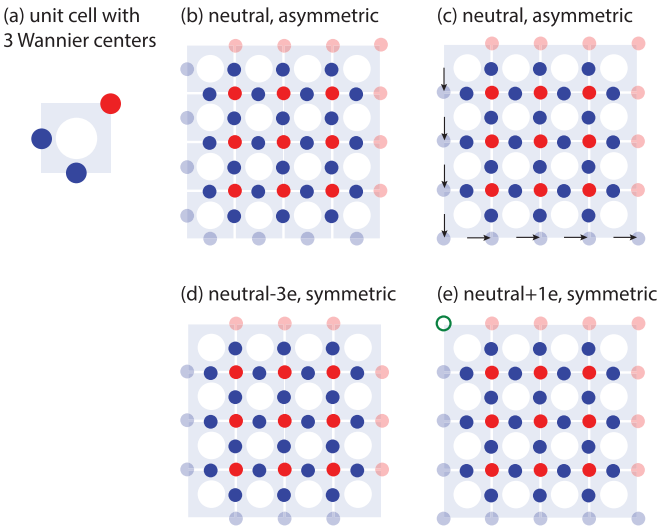

FIG. 5. Filling anomaly in the C_4-symmetric insulator of Eq. (9). (a) A unit cell with charge $3|e|$ at position $1a$ and three electrons with Wannier centers at positions b (red circle) and c, c' (blue circles). (b) A 4×4 lattice formed by tiling the unit cell shown in (a) along x and y. The configuration is neutral but breaks C_4 symmetry. (c) A deformation of (b) as an attempt to restore C_4 symmetry along the edges; symmetry is still broken at corners. (d),(e) Two choices that restore full C_4 symmetry in the lattice by either removing three corner electrons (d) or adding one (e); in either case, charge neutrality is lost.

Let us first illustrate the existence of a corner-induced filling anomaly with an example. Consider Fig. 5, which shows the Wannier centers of the C_4-symmetric crystalline insulator with the Bloch Hamiltonian

$$h^{(4)} = \begin{pmatrix} h_{1b}^{(4)} & \gamma_c \\ \gamma_c^\dagger & h_{2c}^{(4)} \end{pmatrix}. \tag{9}$$

This is an eight-band TCI formed by stacking the primitive generators $h_{1b}^{(4)}$ and $h_{2c}^{(4)}$. γ_c represents any C_4 symmetry-preserving couplings between the generators that do not close the energy band gap. We will enforce a global C_4 symmetry in the lattice of Fig. 5, and consider the four quadrants—each having one corner—as our four symmetry-related sectors. At $\frac{3}{8}$ filling, each unit cell has a positive ionic charge of $3|e|$, and its electrons have Wannier centers at the three maximal Wyckoff positions b, c, and c'. For the choice of Wannier centers at each unit cell shown in Fig. 5(a), a lattice of 4×4 unit cells is shown in Fig. 5(b). Now we show that this TCI must have a charge imbalance caused by the presence of corners if it is to preserve C_4 symmetry: The configuration in Fig. 5(b) preserves C_4 symmetry in the bulk but not at the edges. This configuration, of course, is incompatible. Hence, we deform the edge electrons to procure the preservation of the overall C_4 symmetry, as in Fig. 5(c). We find, however, that C_4 symmetry at the edges can be achieved only at the expense of breaking C_4 symmetry at the corners. To restore the overall C_4 symmetry, we need to cause a charge imbalance by either removing three electrons [Fig. 5(d)] or adding one [open green circle in Fig. 5(e)]. This argument holds for any other choice of deformation of the edges. We conclude that it is not possible to have any choice of Wannier center assignment that preserves charge neutrality and C_4 symmetry simultaneously. The filling anomaly in this case is $\eta = 3$ or $\eta = -1$, and only $\eta \bmod 4 = 3$ is well defined [cf. Eq. (6)]. Since by symmetry the charge has to be equally distributed over each of the four sectors, there has to be a total charge per sector modulo $|e|$ of $Q_{\text{corner}} = \frac{3|e|}{4}$. A plot of the charge density for this insulator (with added intracell hopping terms as detailed in Appendix F in Ref. [61]) is shown in Fig. 1(a). There, we verify that each quadrant has a charge of $\frac{3|e|}{4}$ and that the charges in each quadrant exponentially localize at the corners of the lattice. A more rigorous demonstration of the exponential localization of the corner charge can be found in Appendix H in Ref. [61].

TCIs with $\mathbf{P} \neq (0, 0)$ will have more edge states than the number of edge electrons needed for charge neutrality, with the number of extra edge states scaling with N. As a consequence, a neutral TCI with $\mathbf{P} \neq (0, 0)$ has electrons that delocalize along the boundary in a metallic state and, being gapless, the notion of a corner filling anomaly is lost. Only if $\mathbf{P} = (0, 0)$, will both the bulk and the edges be generically insulating (Appendix F in Ref. [61] shows this characteristic in the simulation of the Hamiltonian in Eq. (9)) allowing for a well-defined corner filling anomaly and consequently well-defined corner charges. Neutrality is then achieved only up to the corner filling anomaly (that does *not* scale with N). Although each of the generators $h_{1b}^{(4)}$ and $h_{2c}^{(4)}$ has $\mathbf{P} = (\frac{e}{2}, \frac{e}{2})$, the combined TCI in Eq. (9) has $\mathbf{P} = (0, 0)$, and therefore its edges are also insulating, leading to the well-defined corner charge of Fig. 1(a).

To generalize the properties illustrated in this example, consider a C_n-symmetric TCI with vanishing polarization forming a lattice in the shape of a regular polygon having m corners, where m is a multiple of n. The vanishing polarization will ensure that all the bulk and edge energy bands below the Fermi level are completely filled. When the filling anomaly is zero, the TCI is neutral, but if it is not, there will be a charge imbalance that localizes at corners. In this second case, the C_n symmetry of the lattice enforces the existence of at least one set of n-fold degenerate states localized at corners. Since the degenerate corner states can be above or below the Fermi level, the total charge imbalance is not unique. We can say at most that the amount of charge robustly protected by the bulk phase is η modulo n [Eq. (6)]. This charge is distributed in equal parts in each of the symmetry-related sectors. Sectors subtended by an angle of $\frac{2\pi}{n}$ rad in our lattices will then have a total (electronic and ionic) charge of

$$Q_{\text{sector}} = \frac{\eta}{n}|e|, \tag{10}$$

which is well-defined only modulo $|e|$. We more generically refer to sectors instead of corners because, depending on the chosen global geometry of the lattice, the charge on a single corner may not be quantized. For example, if a C_2- (C_3-) symmetric bulk Hamiltonian is put on a rectangular (hexagonal) lattice, only the sum of the charges in two adjacent corners will be fractionally quantized. Also, see Ref. [71] for a concrete example of an insulator that has zero filling anomaly and consequently zero total charge at each symmetry-related sector but nevertheless has small residual charges at each corner of opposite sign.

Just as in the case of polarization, the corner filling anomaly comes from the bulk of the crystal. This allows us to also develop a microscopic picture that relates the corner fractional charge in a $\frac{2\pi}{n}$ sector to the local distribution of Wannier centers around corner unit cells. In the extremely dimerized limits (as in the case of our generators, Figs. 2 and 3), the Wannier orbitals are cut in equal parts by the unit cell's boundaries. The fractional number of electrons in a $\frac{2\pi}{n}$ sector (modulo 1) can then be obtained by counting the portion of *bulk* Wannier orbitals falling into the corner unit cells at that sector. Adding symmetry-preserving hopping terms to the Hamiltonian that take it away from the extremely dimerized limit can modify the distribution of Wannier centers in the lattice, with the most dramatic change happening at the corners, and the least change happening near the center of the lattice. This results in the spreading of the corner charge into the bulk with exponentially decreasing amplitude away from the corners (see Appendix H in Ref. [61]). The integrated charge over the $\frac{2\pi}{n}$ sector, however, remains quantized.

This microscopic picture explains the lack of quantization at individual corners—but the strict quantization over symmetry-related sectors—by taking into account the shape of the Wannier orbital. This is discussed in detail in Appendix G in Ref. [61]. Remarkably, this microscopic picture also stipulates the existence of particular cases of C_2-symmetric TCIs that, when put in lattices with four corners, exhibit strict quantization of fractional charge at each individual corner. This is the case of generator $h_{3c}^{(6)}$ when put in a parallelogram lattice, as shown in Appendix G in Ref. [61]. Finally, the microscopic method allows us to assign fractional corner charge even in TCIs with nonvanishing polarization. These corner charges are not physically meaningful on their own, but their value is useful because they can result in well-defined corner charge in combination with other TCIs that make the total polarization vanish. We denote these ill-defined corner charges as *nominal corner charge*; i.e., they are corner charges in systems that also have a bulk polarization. These corner charge values will be useful for the construction of the index theorems for corner charge in Sec. V but cannot be observed unless the polarization is ultimately removed.

V. CONSTRUCTION OF THE TOPOLOGICAL INDICES FOR ELECTRONIC CORNER CHARGE

In Secs. III and IV we saw that the fractionalization of edge and corner charges proceeds from a filling anomaly that is intimately related to the positions of the Wannier centers in C_n-symmetric TCIs. Furthermore, we also saw that the fractional boundary electronic charges can be captured by inspection if we consider electronic configurations in the zero-correlation length limit because then the bulk Wannier centers are located at maximal Wyckoff positions of the lattice even with open boundary conditions.

In order to construct topological indices for the electronic corner charge [akin to those in Eq. (8) for edge charge], we first consider all possible Wannier configurations that respect C_n symmetry in the zero-correlation length limit. This is shown in Fig. 6. The electronic edge and corner charge can then be derived from Fig. 6 pictorially by counting the fraction of Wannier orbitals falling in each unit cell. This information,

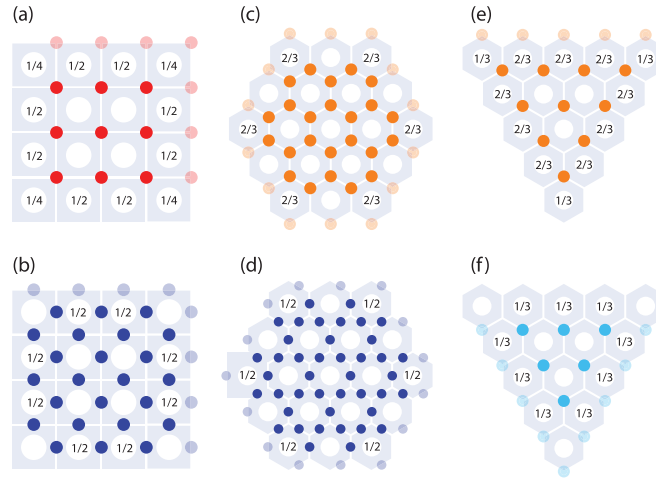

FIG. 6. Edge and corner fractional charges for TCIs with Wannier centers at maximal Wyckoff positions for (a), (b) C_4-symmetric, (c), (d) C_6-symmetric, and (e), (f) C_3-symmetric lattices. (a) One electron at position b of each unit cell. (b) Two electrons at positions c and c'. (c) Two electrons at positions b and b'. (d) Three electrons at positions c, c', and c''. (e) One electron at position b. (f) One electron at position c. Solid colored circles represent bulk electrons; dimmed colored circles represent boundary electrons for a particular choice of C_n-symmetry breaking; white circles represent atomic ions. Bulk unit cells are always neutral. Electronic charges at edge and corner unit cells after the removal of the symmetry breaking electrons are indicated mod 1 (in units of the electron charge e).

along with the Wannier center description of the primitive generators defined in Sec. II, allows us to then extract both the electronic edge and corner charges of each generator, which we will need to construct the topological indices for the quanta of charge at corners.

In what follows, we consider all minimal and inequivalent Wannier configurations given a C_n crystalline symmetry (by minimal we mean that we will put only one Wannier orbital at each Wyckoff position). In C_4-symmetric TCIs, there are two possible Wannier configurations, one with one Wannier orbital at Wyckoff position b [Fig. 6(a)] and a second one with two Wannier orbitals, one at c and another one at c' [Fig. 6(b)]. Both configurations have polarization $\mathbf{P} = (\frac{e}{2}, \frac{e}{2})$, leading to the fractional charge on the edges. However, when we consider corners, a crucial distinction emerges; Wannier orbitals at Wyckoff positions b have fractional corner charge of $\frac{e}{4}$, while those at positions c, c' have no expected fractional corner charge. For C_2-symmetric TCIs, in addition to the two configurations allowed for C_4-symmetric TCIs, there is a third configuration having one Wannier orbital at Wyckoff positions d (not pictured), which render $\frac{e}{2}$ edge charge along one pair of edges due to $\mathbf{P} = (0, \frac{e}{2})$, but no corner charge. For C_6-symmetric TCIs, there are two configurations, both having $\mathbf{P} = (0, 0)$, and consequently leading to a vanishing edge charge. At corners, however, the charge is fractionalized. The first configuration has two Wannier orbitals, one at Wyckoff positions b and another one at b' [Fig. 6(c)]. This configuration leads to corner charge in multiples of $\frac{2e}{3}$. The second configuration has three Wannier orbitals, each of them at Wyckoff positions c, c' and c'', respectively [Fig. 6(d)]. This

TABLE I. Topological invariants, polarization $\mathbf{P}$, and nominal electronic corner charge of the primitive generators that span the classifications of C_n-symmetric TCIs. The values of $\mathbf{P} = p_1\mathbf{a_1} + p_2\mathbf{a_2}$ are given in pairs (p_1, p_2). The unit lattice vectors are $\mathbf{a_1} = \hat{\mathbf{x}}$, $\mathbf{a_2} = \hat{\mathbf{y}}$ for C_4 and C_2-symmetric lattices, and $\mathbf{a_1} = \hat{\mathbf{x}}$, $\mathbf{a_2} = \frac{1}{2}\hat{\mathbf{x}} + \frac{\sqrt{3}}{2}\hat{\mathbf{y}}$ for C_3 and C_6-symmetric lattices.

Symm.	Generator	Invariants			$\mathbf{P}$	Q_{corner}
		$[X_1^{(2)}]$	$[M_1^{(4)}]$	$[M_2^{(4)}]$		
C_4	$h_{1b}^{(4)}$	-1	1	0	$(\frac{e}{2}, \frac{e}{2})$	$\frac{e}{4}$
	$h_{2b}^{(4)}$	2	0	0	(0,0)	$\frac{e}{2}$
	$h_{2c}^{(4)}$	1	1	-1	$(\frac{e}{2}, \frac{e}{2})$	0
		$[X_1^{(2)}]$	$[Y_1^{(2)}]$	$[M_1^{(2)}]$		
C_2	$h_{1b}^{(4)}$	-1	-1	0	$(\frac{e}{2}, \frac{e}{2})$	$\frac{e}{2}$
	$h_{2c}^{(4)}$	1	1	2	$(\frac{e}{2}, \frac{e}{2})$	0
	$h_{1d}^{(2)}$	0	1	1	$(0, \frac{e}{2})$	0
		$[M_1^{(2)}]$	$[K_1^{(3)}]$			
C_6	$h_{4b}^{(6)}$	0	2		(0,0)	$\frac{e}{3}$
	$h_{3c}^{(6)}$	2	0		(0,0)	$\frac{e}{2}$
		$[K_1^{(3)}]$	$[K_2^{(3)}]$			
C_3	$h_{2b}^{(3)}$	1	-1		$(\frac{e}{3}, \frac{e}{3})$	$\frac{2e}{3}$
	$h_{2c}^{(3)}$	1	0		$(\frac{2e}{3}, \frac{2e}{3})$	0

second configuration leads to corner charge in multiples of $\frac{e}{2}$. The combination of these two systems can consequently give rise to corner charge in multiples of $\frac{e}{6}$. In C_3-symmetric TCIs, there are also two configurations: one with one Wannier orbital at Wyckoff positions b [Fig. 6(e)] and a second one with Wannier orbital at c [Fig. 6(f)]. They have polarizations of $\mathbf{P} = (\frac{2e}{3}, \frac{2e}{3})$ and $\mathbf{P} = (\frac{e}{3}, \frac{e}{3})$, respectively. Both configurations then give rise to the edge charge. At corners, however, the configuration with one Wannier orbital at Wyckoff position b does not have fractional charges, while the one having the Wannier orbital at c does. By these considerations, the *nominal electronic corner charge* for the primitive generators are found to be those in Table I.

This information characterizes the corner properties of TCIs in class AI having additional C_n symmetry and hence allows us to build index theorems that determine the fractional electronic corner charge. This relies on the fact that for a Hamiltonian $h_3^{(n)} = h_1^{(n)} \oplus h_2^{(n)}$, (i) its boundary electronic charge is $Q_3 = Q_1 + Q_2$ (mod e) and (ii) its invariants are $\chi_3^{(n)} = \chi_1^{(n)} + \chi_2^{(n)}$. The index for the electronic corner charge of a C_n-symmetric insulator is then given by a linear combination of the invariants that form the vector $\chi^{(n)}$. For example, C_4-symmetric TCIs have three invariants. The electronic corner charge is given by $Q_{\text{corner}}^{(4)} = \alpha_1[X_1^{(2)}] + \alpha_2[M_1^{(4)}] + \alpha_3[M_2^{(4)}]$. To find the coefficients $\alpha_{i=1,2,3}$, we solve for $Q_i = \chi_{ij}^{(4)}\alpha_j$, where Q_i is the ith element in the vector of corner charges formed by the last column in Table I, and $\chi_{ij}^{(4)}$ is the (i, j)th element in the matrix formed by the three columns labeled $[X_1^{(2)}]$, $[M_1^{(4)}]$, and $[M_2^{(4)}]$ in Table I. This approach gives

$$
\begin{aligned}
Q_{\text{corner}}^{(4)} &= \frac{e}{4}\left([X_1^{(2)}] + 2[M_1^{(4)}] + 3[M_2^{(4)}]\right) \mod e \\
Q_{\text{corner}}^{(2)} &= \frac{e}{4}\left(-[X_1^{(2)}] - [Y_1^{(2)}] + [M_1^{(2)}]\right) \mod e \\
Q_{\text{corner}}^{(6)} &= \frac{e}{4}[M_1^{(2)}] + \frac{e}{6}[K_1^{(3)}] \mod e \\
Q_{\text{corner}}^{(3)} &= \frac{e}{3}[K_2^{(3)}] \mod e,
\end{aligned}
\tag{11}
$$

where the superindex n in $Q_{\text{corner}}^{(n)}$ labels the C_n symmetry. In the C_n-symmetric classification, $Q_{\text{corner}}^{(n)}$ is a $\mathbb{Z}_n$ topological index. We could refer to the indices in Eq. (11) as *secondary topological indices* because they require the primary topological index—the polarization $\mathbf{P}$—to vanish in order to give a protected, corner-localized quantized feature.

As an example of the application of the indices in Eq. (11), let us return to the eight-band model considered above in Eq. (9), which has electronic corner charge of $\frac{e}{4}$, and a total (electronic *and* ionic) charge density shown in Fig. 1(a). By itself, the model $h_{1b}^{(4)}$ at $\frac{1}{4}$ filling that forms one block of the eight band system has edge states owing to its $\mathbf{P} = (\frac{e}{2}, \frac{e}{2})$ polarization. Not all the edge states can be occupied at this filling while preserving the symmetry, however, and the edge is generically metallic (see Appendix F in Ref. [61] for details). We can remove the polarization by the addition of $h_{2c}^{(4)}$, the second block of the eight band model, which at $\frac{1}{2}$ filling also has $\mathbf{P} = (\frac{e}{2}, \frac{e}{2})$. Under any C_4 symmetry-preserving coupling terms γ_c that keep the energy gap open, the primary index of the combined insulator [Eq. (9)] at $\frac{3}{8}$ filling is $\mathbf{P} = (0, 0)$, but its secondary index is $Q_{\text{corner}}^{(4)} = \frac{e}{4}$ [first equation in Eq. (11)]. To confirm that this charge is generically stable, we add general random hopping terms to the Hamiltonian up to nearest-neighbor unit cells that preserve only TRS and C_4 symmetry and numerically verify that the $\frac{e}{4}$ electronic charge remains strictly quantized (see Appendix F in Ref. [61]). In contrast, if we add perturbations that break C_4 symmetry down to C_2 symmetry (C_2 symmetry keeps bulk polarization quantized to zero), the quantization of charge at each corner in the lattice is lost. However, the sum of electronic corner charge of two adjacent corners (i.e., in a region covering half the lattice) is $\frac{e}{2}$, in agreement with the value predicted by the secondary index in the second equation of Eq. (11).

The indices in Eq. (11) can be used to generate other corner charges. The total (ionic and electronic) fractional charge of $\frac{|e|}{2}$ in Fig. 1(b) was obtained with a Hamiltonian deformable to $h_{1b}^{(4)} \oplus h_{1b}^{(4)}$ at $\frac{1}{4}$ filling, while the corner charges of $\frac{|e|}{6}$ and $\frac{|e|}{3}$ in Figs. 1(c) and 1(d) were obtained by Hamiltonians deformable to $h_{4b}^{(6)} \oplus h_{3c}^{(6)}$ at $\frac{7}{12}$ filling and to $h_{2b}^{(3)} \oplus h_{2c}^{(3)}$ at $\frac{2}{3}$ filling, respectively. In all cases, the polarization of the Hamiltonians is $\mathbf{P} = (0, 0)$, and the electronic corner charge indices in Eq. (11) give $Q_{\text{corner}} = \frac{e}{2}$, $\frac{5e}{6}$, and $\frac{2e}{3}$, respectively. The total charge density, which takes into account the ionic contributions, results in the fractional charges shown in Fig. 1. Since the electronic charge fractionalization is a property of the bulk, a fast way to determine the filling anomaly is to remove all boundary Wannier centers in the lattice

TABLE II. Charge imbalance (upon removal of all boundary Wannier centers), filling anomaly η [Eq. (6)], and total sector charge Q [Eq. (10)] for some models having vanishing bulk polarization. Calculations are assuming that C_n-symmetric Bloch Hamiltonians are put in C_n-symmetric lattices, respectively. N is the number of unit cells per edge.

Insulator	Charge imbalance	η	Q_{sector}
$h^{(4)}_{1b} \oplus h^{(4)}_{2c}$	$4N-1$	3	$\frac{3\lvert e\rvert}{4}$
$h^{(4)}_{1b} \oplus h^{(4)}_{1b}$	$4N-2$	2	$\frac{\lvert e\rvert}{2}$
$h^{(6)}_{4b}$	$6N-4$	2	$\frac{\lvert e\rvert}{3}$
$h^{(6)}_{3c}$	$6N-3$	3	$\frac{\lvert e\rvert}{2}$
$h^{(3)}_{2b} \oplus h^{(3)}_{2c}$	$6N-2$	1	$\frac{\lvert e\rvert}{3}$

(e.g., removing all dimmed circles in Fig. 5). The resulting charge imbalance mod n then gives the filling anomaly. Table II shows the charge imbalance by removal of all boundary Wannier centers, filling anomalies, and total (electronic and ionic) corner charge values over $\frac{2\pi}{n}$ spatial sectors for C_n-symmetric TCIs used in the simulations in Fig. 1.

VI. FRACTIONAL CORNER CHARGE IN TCIS WITHOUT A WANNIER REPRESENTATION

The secondary index theorems in Eq. (11) were derived using a basis of primitive generators that admit Wannier representations. We chose that basis to make transparent the derivation of the indices. However, the indices themselves transcend the basis and indicate the fractionalization of electronic corner charge even in TCIs that are not Wannier representable, for example, in fragile TCIs [46–49]. Recently, corner states and corner fractional charges have been found in fragile TCIs [27,33,40,41], and the existence of this fractionalization has been associated with quantized nested Berry phases [27,33,40,41] originally proposed in Ref. [14] for the characterization of corner charges in quantized quadrupole insulators. Unlike atomic insulators, fragile TCIs do not admit the construction of Wannier centers. However, they have the property that upon the addition of atomic TCIs, the combined system becomes Wannier representable. We can write this relation as $H_{AI_2} \sim H_{FT} \oplus H_{AI_1}$, where $AI_{i=1,2}$ are atomic TCIs and FT is the fragile TCI. The electronic corner charges of these TCIs must then obey $Q_{AI_2} = Q_{FT} + Q_{AI_1}$, which implies that, since both Q_{AI_1} and Q_{AI_2} are quantized, Q_{FT} will also be quantized. Moreover, due to the algebraic structure of our classification [52,53], it follows that the classes of these TCIs in their C_n classification obey $\chi^{(n)}_{AI_2} = \chi^{(n)}_{FT} + \chi^{(n)}_{AI_1}$. The same algebraic structure stipulates that the secondary indices must obey $Q^{(n)}_{\text{corner}}(\chi^{(n)}_{AI_2}) = Q^{(n)}_{\text{corner}}(\chi^{(n)}_{FT}) + Q^{(n)}_{\text{corner}}(\chi^{(n)}_{AI_1})$. Since for the atomic TCIs we know that $Q^{(n)}_{\text{corner}}(\chi^{(n)}_{AI_i}) = Q_{AI_i}$, for $i = 1, 2$, it follows that $Q^{(n)}_{\text{corner}}(\chi^{(n)}_{FT}) = Q_{FT}$. Thus, our indices in Eq. (11) correctly determine the quantization of electronic fractional charge in fragile phases. A concrete example of the corner charge in a fragile phase is shown in Appendix I in Ref. [61] for one of the phases described in the recent preprint of Ref. [72]. There, we (i) calculate the indices from a decomposition into atomic TCIs, (ii) directly evaluate the secondary index from the topological invariants of the fragile phase, and (iii) compare these results with numerical simulations.

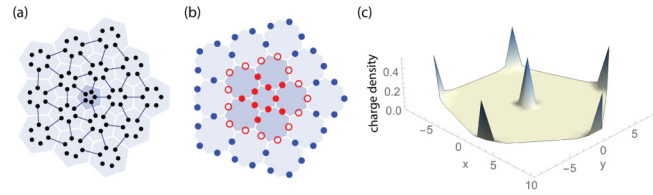

FIG. 7. Quantized fractionalization of charge at the core of disclinations. (a) Disclination in the lattice of primitive generator $h^{(6)}_{3c}$. (b) Wannier centers for the lattice in (a). There is an overall fractional electronic charge (each hollow circle contributes $\frac{e}{2}$ charge) within the region of darker unit cells which enclose the core of the disclination. (c) Charge density for the disclination in (a). All corners and the core of the disclination have charges of $\frac{|e|}{2}$. The simulation is done over 276 unit cells with added intra-unit cell hoppings between nearest neighbors of $\frac{1}{4}$ the amplitude of the interunit cell hoppings.

VII. FRACTIONAL CHARGE AT TOPOLOGICAL DEFECTS

First-order TCIs manifest fractional charges at dislocations, following the topological index $Q_{\text{dislocation}} = \frac{1}{2\pi}\mathbf{G}_v \cdot \mathbf{B}$, where $\mathbf{G}_v$ is the weak topological index related to the polarization $\mathbf{P}$, Eq. (1), and $\mathbf{B}$ is the Burgers vector that characterizes the dislocation [67]. Higher-order TCIs have $\mathbf{P} = \mathbf{0}$ and thus do not manifest fractional charges at dislocations. In this section we will see that instead they manifest fractional charges at the core of disclinations. Indeed, it is known that topological disclination defects that induce a curvature singularity in the lattice of C_n-symmetric topological superconductors can trap Majorana bound states [52,53]. Here, we find that these defects also trap fractional charges in higher-order TCIs. In Fig. 7 we show a disclination with a Frank angle of $-\frac{2\pi}{6}$ rad in the primitive model $h^{(6)}_{3c}$. Inducing such a disclination converts the hexagon of Fig. 3(d) into the pentagon of Fig. 7(a). The five corners in the pentagon give rise to an overall corner charge of $\frac{5e}{2}$. Thus, the core of the disclination must trap a fractional charge of $\frac{e}{2}$. Indeed, the Wannier center configuration shown in Fig. 7(b) for the lattice in Fig. 7(a) reveals that, for any area comprised of unit cells containing the core of the disclination, a total fractional number of electrons is enclosed. Figure 7(c) shows a plot of the charge density for the lattice in Fig. 7(a) but to which additional hopping terms inside the unit cell were added of weak enough amplitude so as to not cause a phase transition. This plot indeed presents the expected charge distribution. If the intra-unit cell couplings are larger than the interunit cell couplings, a bulk phase transition occurs, leading to vanishing corner charges and integer charge at the core of the disclination.

Generalizing this principle of charge conservation (mod $|e|$), our corner charge indices can be immediately used to generate indices for the fractional charge at the core of

disclinations in a C_n-symmetric insulator:

$$Q_{\text{disclination}} = -\frac{\Omega}{2\pi/n} Q_{\text{corner}} \mod |e|. \tag{12}$$

We also note that inducing this disclination disrupts the chiral symmetry in the primitive model $h^{(6)}_{3c}$. Thus, although the pristine insulator has zero energy states localized at corners [21], there are no such states at the core of the disclination. Despite this, the fractional charge trapped at the core of the defect is robustly quantized to $\frac{e}{2}$, suggesting that disclinations are bulk probes of TCIs with $Q^{(n)}_{\text{corner}} \neq 0$ [52,53,73–75], just as dislocations are bulk probes of TCIs with $\mathbf{P} \neq \mathbf{0}$ [67,75–81].

VIII. DISCUSSION AND CONCLUSION

In this paper, we have shown that electronic charge fractionalizes in multiples of $\frac{e}{n}$ at the corners of C_n symmetric TCIs with vanishing polarization. We built topological indices for the quanta of corner charge in terms of the band representations at high symmetry points of the Brillouin zone. These constitute *secondary topological indices*, Eq. (11), that signal the presence of higher order topology in TCIs with vanishing polarization. When TCIs admit a Wannier representation, we find an clear relation between the existence of fractional corner charge and the positions of the Wannier centers in the bulk of the crystal. More generally, however, a Wannier representation is not guaranteed, but a filling anomaly can still persist, which in turn robustly protects the fractionalization of corner charge. Since the fractionalization of corner charge is ultimately related to the Wannier centers of the electrons within the crystal, we anticipate that the same principles derived in this study will lead to the characterization of corner charge in other classes of the tenfold classification. For example, adding spin will double the corner charge quantization due to Kramers' degeneracy. However, deriving index theorems in these classes will not be as straightforward because symmetry representations at high symmetry points do not suffice to determine the Wannier centers in spinful systems.

In practice, we expect solid state TCIs with nonzero $Q^{(n)}_{\text{corner}}$ indices to prefer to be neutral. Despite the overall neutrality, we still expect the corner charges to be observable. The excess or deficit charge could be compensated for in several ways. In any realistic crystal, there will be impurities and, since the filling anomaly due to corners only indicates $O(1)$ uncompensated charges, impurities could absorb the charges needed to realize neutrality. This will affect the corner charge at most by an integer when the impurity is localized very near the corner and thus the fractional part of the charge will be preserved. Another scenario for localized charges is in TCIs with midgap topological modes associated with the fractional charge. In these systems, the symmetry could be mildly broken explicitly or spontaneously, allowing for a ground state filling of the midgap modes that is globally neutral. Then, the corner charges will also be shifted by an integer and the fractional portion of the charge is undisturbed. If instead there are no midgap topological or impurity states, we could imagine that the overall excess charge at the corners can be compensated by an occupation/de-occupation of eigenstates in the conduction or valence bulk bands. The resulting effect is a near-to-quantized corner charge, with a bulk interior containing the opposite charge, as shown in Appendix J in Ref. [61]. The corrections to both the corner charge and the background bulk charge scale as $O(1/N^2)$ for a lattice with N unit cells per side and thus closely approximate exact quantization in the thermodynamic limit.

While we expect there to be electronic material realizations of systems with fractional corner charges, we believe that the most straightforward realization of our models is in metamaterial systems. Since our classifications are for spinless systems that preserve time-reversal symmetry, the hopping terms in the Hamiltonian do not require any additional phase factors and can be engineered using only evanescently coupled modes. Thus, our generators can be easily implemented in a wide range of metamaterial platforms, as in the works in Refs. [21,25,26,82–84]. In the experiments in Refs. [21,82–84], the expected corner properties were observed spectroscopically through the appearance of corner states protected to be at midgap by chiral symmetry, $\Pi h(\mathbf{k}) = -h(\mathbf{k})\Pi$, for some chiral operator Π. We illustrated here, however, that the true signature of fractionalization of corner charge is a bulk topological property of the subspace of occupied bands, and does not need to manifest in connection with corner-localized midgap states. In the absence of midgap states, more sophisticated experiments, for example, exploring the spatial distribution of all the states in an energy band, can reveal the fractional signatures at corners even in metamaterials. Such experiments could easily explore the properties of disclinations as well by introducing such defects in resonator arrays or photonic crystals.

ACKNOWLEDGMENTS

We thank Aris Alexandradinata, B. Andrei Bernevig, Eugeniu Plamadeala, Emil Prodan, and Benjamin Wieder for useful discussions. In particular, we thank Andrei Bernevig and Benjamin Wieder for detailed discussion and for sharing their manuscript, Ref. [41], during the preparation of this paper. W.A.B. thanks the support of the Eberly Postdoctoral Fellowship at the Pennsylvania State University. W.A.B. and T.L.H. thank the US National Science Foundation under Grant No. DMR-1351895 and the Sloan Foundation for support. T.L. thanks US National Science Foundation (NSF) Emerging Frontiers in Research and Innovation (EFRI) Grant No. EFMA-1627184.

[1] J. C. Y. Teo, L. Fu, and C. L. Kane, Surface states and topological invariants in three-dimensional topological insulators: Application to $Bi_{1-x}Sb_x$, Phys. Rev. B **78**, 045426 (2008).

[2] L. Fu, Topological Crystalline Insulators, Phys. Rev. Lett. **106**, 106802 (2011).

[3] T. H. Hsieh, H. Lin, J. Liu, W. Duan, A. Bansil, and L. Fu, Topological crystalline insulators in the SnTe material class, Nat. Commun. **3**, 982 (2012).

[4] R.-J. Slager, A. Mesaros, V. Juricic, and J. Zaanen, The space group classification of topological band-insulators, Nat. Phys. **9**, 98 (2013).

[5] K. Shiozaki and M. Sato, Topology of crystalline insulators and superconductors, Phys. Rev. B **90**, 165114 (2014).

[6] C. Fang and L. Fu, New classes of three-dimensional topological crystalline insulators: Nonsymmorphic and magnetic, Phys. Rev. B **91**, 161105(R) (2015).

[7] H. Watanabe and L. Fu, Topological crystalline magnets: Symmetry-protected topological phases of fermions, Phys. Rev. B **95**, 081107(R) (2017).

[8] J. Zak, Berry's Phase for Energy Bands in Solids, Phys. Rev. Lett. **62**, 2747 (1989).

[9] R. D. King-Smith and D. Vanderbilt, Theory of polarization of crystalline solids, Phys. Rev. B **47**, 1651 (1993).

[10] D. Vanderbilt and R. D. King-Smith, Electric polarization as a bulk quantity and its relation to surface charge, Phys. Rev. B **48**, 4442 (1993).

[11] R. Resta, Macroscopic polarization in crystalline dielectrics: The geometric phase approach, Rev. Mod. Phys. **66**, 899 (1994).

[12] T. L Hughes, E. Prodan, and B. A. Bernevig, Inversion-symmetric topological insulators, Phys. Rev. B **83**, 245132 (2011).

[13] A. M. Turner, Y. Zhang, R. S. K. Mong, and A. Vishwanath, Quantized response and topology of magnetic insulators with inversion symmetry, Phys. Rev. B **85**, 165120 (2012).

[14] W. A. Benalcazar, B. A. Bernevig, and T. L. Hughes, Quantized electric multipole insulators, Science **357**, 61 (2017).

[15] W. A. Benalcazar, B. A. Bernevig, and T. L. Hughes, Electric multipole moments, topological multipole moment pumping, and chiral hinge states in crystalline insulators, Phys. Rev. B **96**, 245115 (2017).

[16] Chen Fang and Liang Fu, Rotation anomaly and topological crystalline insulators, arXiv:1709.01929.

[17] Zhida Song, Zhong Fang, and Chen Fang, $(d-2)$-Dimensional Edge States of Rotation Symmetry Protected Topological States, Phys. Rev. Lett. **119**, 246402 (2017).

[18] J. Langbehn, Y. Peng, L. Trifunovic, F. von Oppen, and P. W. Brouwer, Reflection-Symmetric Second-Order Topological Insulators and Superconductors, Phys. Rev. Lett. **119**, 246401 (2017).

[19] F. Schindler, A. M. Cook, M. G. Vergniory, Z. Wang, S. S. P. Parkin, B. A. Bernevig, and T. Neupert, Higher-order topological insulators, Sci. Adv. **4**, eaat0346 (2018).

[20] L. Trifunovic and P. W. Brouwer, Higher-Order Bulk-Boundary Correspondence for Topological Crystalline Phases, Phys. Rev. X **9**, 011012 (2019).

[21] J. Noh, W. A. Benalcazar, S. Huang, M. J. Collins, K. P. Chen, T. L. Hughes, and M. C. Rechtsman, Topological protection of photonic mid-gap defect modes, Nat. Photon. **12**, 408 (2018).

[22] M. Ezawa, Higher-Order Topological Insulators and Semimetals on the Breathing Kagome and Pyrochlore Lattices, Phys. Rev. Lett. **120**, 026801 (2018).

[23] G. van Miert and C. Ortix, Higher-order topological insulators protected by inversion and rotoinversion symmetries, Phys. Rev. B **98**, 081110(R) (2018).

[24] Bi-Ye Xie, Hong-Fei Wang, Hai-Xiao Wang, Xue-Yi Zhu, Jian-Hua Jiang, Ming-Hui Lu, and Yan-Feng Chen, Second-order photonic topological insulator with corner states, Phys. Rev. B **98**, 205147 (2018).

[25] X. Ni, M. Weiner, A. Alù, and A. B. Khanikaev, Observation of higher-order topological acoustic states protected by generalized chiral symmetry, Nat. Mater. **18**, 113 (2019).

[26] H. Xue, Y. Yang, F. Gao, Yidong Chong, and B. Zhang, Acoustic higher-order topological insulator on a kagome lattice, Nat. Mater. **18**, 108 (2019).

[27] Junyeong Ahn, Sungjoon Park, and Bohm-Jung Yang, Failure of Nielsen-Ninomiya Theorem and Fragile Topology in Two-Dimensional Systems with Space-Time Inversion Symmetry: Application to Twisted Bilayer Graphene at Magic Angle, Phys. Rev. X **9**, 021013 (2019).

[28] M. Ezawa, Magnetic second-order topological insulators and semimetals, Phys. Rev. B **97**, 155305 (2018).

[29] M. Ezawa, Strong and weak second-order topological insulators with hexagonal symmetry and $\mathbb{Z}_3$ index, Phys. Rev. B **97**, 241402(R) (2018).

[30] M. Ezawa, Topological Switch between Second-Order Topological Insulators and Topological Crystalline Insulators, Phys. Rev. Lett. **121**, 116801 (2018).

[31] F. K. Kunst, G. van Miert, and E. J. Bergholtz, Lattice models with exactly solvable topological hinge and corner states, Phys. Rev. B **97**, 241405(R) (2018).

[32] S. Franca, J. van den Brink, and I. C. Fulga, Anomalous higher-order topological insulators, Phys. Rev. B **98**, 201114(R) (2018).

[33] Z. Wang, B. J. Wieder, J. Li, B. Yan, and B. A. Bernevig, Higher-order topology, monopole nodal lines, and the origin of large Fermi Arcs in transition metal dichalcogenides XTe_2 (X = Mo, W), arXiv:1806.11116.

[34] A. Matsugatani and H. Watanabe, Connecting higher-order topological insulators to lower-dimensional topological insulators, Phys. Rev. B **98**, 205129 (2018).

[35] F. Schindler, Z. Wang, M. G. Vergniory, A. M. Cook, A. Murani, S. Sengupta, A. Yu. Kasumov, R. Deblock, S. Jeon, I. Drozdov, H. Bouchiat, S. Guéron, A. Yazdani, B. A. Bernevig, and T. Neupert, Higher-order topology in bismuth, Nat. Phys. **14**, 918 (2018).

[36] E. Khalaf, H. C. Po, A. Vishwanath, and H. Watanabe, Symmetry Indicators and Anomalous Surface States of Topological Crystalline Insulators, Phys. Rev. X **8**, 031070 (2018).

[37] E. Khalaf, Higher-order topological insulators and superconductors protected by inversion symmetry, Phys. Rev. B **97**, 205136 (2018).

[38] Y. You, T. Devakul, F. J. Burnell, and T. Neupert, Higher-order symmetry-protected topological states for interacting bosons and fermions, Phys. Rev. B **98**, 235102 (2018).

[39] N. Varnava and D. Vanderbilt, Surfaces of axion insulators, Phys. Rev. B **98**, 245117 (2018).

[40] B. J. Wieder and B. A. Bernevig, The axion insulator as a pump of fragile topology, arXiv:1810.02373.

[41] B. J. Wieder, Z. Wang, J. Cano, X. Dai, L. M. Schoop, B. Bradlyn, and B. A. Bernevig (unpublished).

[42] S. Kivelson, Wannier functions in one-dimensional disordered systems: Application to fractionally charged solitons, Phys. Rev. B **26**, 4269 (1982).

[43] G. van Miert and C. Ortix, Excess charges as a probe of one-dimensional topological crystalline insulating phases, Phys. Rev. B **96**, 235130 (2017).

[44] J.-W. Rhim, J. Behrends, and J. H. Bardarson, Bulk-boundary correspondence from the intercellular Zak phase, Phys. Rev. B **95**, 035421 (2017).

[45] B. Bradlyn, L. Elcoro, J. Cano, M. G. Vergniory, Zhijun Wang, C. Felser, M. I. Aroyo, and B. A. Bernevig, Topological quantum chemistry, Nature (London) **547**, 298 (2017).

[46] Hoi Chun Po, H. Watanabe, and A. Vishwanath, Fragile Topology and Wannier Obstructions, Phys. Rev. Lett. **121**, 126402 (2018).

[47] J. Cano, B. Bradlyn, Z. Wang, L. Elcoro, M. G. Vergniory, C. Felser, M. I. Aroyo, and B. A. Bernevig, Topology of Disconnected Elementary Band Representations, Phys. Rev. Lett. **120**, 266401 (2018).

[48] A. Bouhon, A. M. Black-Schaffer, and R.-J. Slager, Wilson loop approach to metastable topology of split elementary band representations and topological crystalline insulators with time reversal symmetry, arXiv:1804.09719.

[49] B. Bradlyn, Zhijun Wang, J. Cano, and B. A. Bernevig, Disconnected elementary band representations, fragile topology, and Wilson loops as topological indices: An example on the triangular lattice, Phys. Rev. B **99**, 045140 (2019).

[50] C. Fang, M. J. Gilbert, and B. A. Bernevig, Bulk topological invariants in noninteracting point group symmetric insulators, Phys. Rev. B **86**, 115112 (2012).

[51] C. Fang, M. J. Gilbert, and B. A. Bernevig, Entanglement spectrum classification of C_n-invariant noninteracting topological insulators in two dimensions, Phys. Rev. B **87**, 035119 (2013).

[52] J. C. Y. Teo and T. L. Hughes, Existence of Majorana-Fermion Bound States on Disclinations and the Classification of Topological Crystalline Superconductors in Two Dimensions, Phys. Rev. Lett. **111**, 047006 (2013).

[53] W. A. Benalcazar, J. C. Y. Teo, and T. L. Hughes, Classification of two-dimensional topological crystalline superconductors and Majorana bound states at disclinations, Phys. Rev. B **89**, 224503 (2014).

[54] R. Resta, Quantum-Mechanical Position Operator in Extended Systems, Phys. Rev. Lett. **80**, 1800 (1998).

[55] Rui Yu, Xiao Liang Qi, Andrei Bernevig, Zhong Fang, and Xi Dai, Equivalent expression of $\mathbb{Z}_2$ topological invariant for band insulators using the non-Abelian Berry connection, Phys. Rev. B **84**, 075119 (2011).

[56] A. Alexandradinata, X. Dai, and B. A. Bernevig, Wilson-loop characterization of inversion-symmetric topological insulators, Phys. Rev. B **89**, 155114 (2014).

[57] J. Cano, B. Bradlyn, Z. Wang, L. Elcoro, M. G. Vergniory, C. Felser, M. I. Aroyo, and B. A. Bernevig, Building blocks of topological quantum chemistry: Elementary band representations, Phys. Rev. B **97**, 035139 (2018).

[58] A. Altland and M. R. Zirnbauer, Nonstandard symmetry classes in mesoscopic normal-superconducting hybrid structures, Phys. Rev. B **55**, 1142 (1997).

[59] A. P. Schnyder, S. Ryu, A. Furusaki, and A. W. W. Ludwig, Classification of topological insulators and superconductors in three spatial dimensions, Phys. Rev. B **78**, 195125 (2008).

[60] A. Kitaev, Periodic table for topological insulators and superconductors, AIP Conf. Proc. **1134**, 22 (2009).

[61] See Supplemental Material at http://link.aps.org/supplemental/10.1103/PhysRevB.99.245151 for complete derivations.

[62] R. Resta, Theory of the electric polarization in crystals, Ferroelectrics **136**, 51 (1992).

[63] R. Resta, M. Posternak, and A. Baldereschi, Towards a Quantum Theory of Polarization in Ferroelectrics: The Case of $knbo_3$, Phys. Rev. Lett. **70**, 1010 (1993).

[64] R. Resta and D. Vanderbilt, Theory of polarization: A modern approach, in *Physics of Ferroelectrics: A Modern Perspective* (Springer, Berlin, Heidelberg, 2007), pp. 31–68.

[65] J. Kruthoff, J. de Boer, J. van Wezel, C. L. Kane, and R.-J. Slager, Topological Classification of Crystalline Insulators through Band Structure Combinatorics, Phys. Rev. X **7**, 041069 (2017).

[66] Hoi Chun Po, A. Vishwanath, and H. Watanabe, Symmetry-based indicators of band topology in the 230 space groups, Nat. Commun. **8**, 50 (2017).

[67] J. C. Y. Teo and C. L. Kane, Topological defects and gapless modes in insulators and superconductors, Phys. Rev. B **82**, 115120 (2010).

[68] N. Marzari and D. Vanderbilt, Maximally localized generalized wannier functions for composite energy bands, Phys. Rev. B **56**, 12847 (1997).

[69] N. Marzari, A. A. Mostofi, J. R. Yates, I. Souza, and D. Vanderbilt, Maximally localized wannier functions: Theory and applications, Rev. Mod. Phys. **84**, 1419 (2012).

[70] W. P. Su, J. R. Schrieffer, and A. J. Heeger, Solitons in Polyacetylene, Phys. Rev. Lett. **42**, 1698 (1979).

[71] Y. Zhou, K. M. Rabe, and D. Vanderbilt, Surface polarization and edge charges, Phys. Rev. B **92**, 041102(R) (2015).

[72] S. Liu, A. Vishwanath, and E. Khalaf, Shift insulators: rotation-protected two-dimensional topological crystalline insulators, arXiv:1809.01636.

[73] A. Rüegg and C. Lin, Bound States of Conical Singularities in Graphene-Based Topological Insulators, Phys. Rev. Lett. **110**, 046401 (2013).

[74] A. Rüegg, S. Coh, and J. E. Moore, Corner states of topological fullerenes, Phys. Rev. B **88**, 155127 (2013).

[75] J. C.Y. Teo and T. L. Hughes, Topological defects in symmetry-protected topological phases, Annu. Rev. Condens. Matter Phys. **8**, 211 (2017).

[76] Ying Ran, Yi Zhang, and A. Vishwanath, One-dimensional topologically protected modes in topological insulators with lattice dislocations, Nat. Phys. **5**, 298 (2009).

[77] Y. Ran, Weak indices and dislocations in general topological band structures, arXiv:1006.5454.

[78] V. Juričić, A. Mesaros, R.-J. Slager, and J. Zaanen, Universal Probes of Two-Dimensional Topological Insulators: Dislocation and π Flux, Phys. Rev. Lett. **108**, 106403 (2012).

[79] S. Gopalakrishnan, J. C. Y. Teo, and T. L. Hughes, Disclination Classes, Fractional Excitations, and the Melting of Quantum Liquid Crystals, Phys. Rev. Lett. **111**, 025304 (2013).

[80] T. L. Hughes, Hong Yao, and Xiao-Liang Qi, Majorana zero modes in dislocations of Sr_2RuO_4, Phys. Rev. B **90**, 235123 (2014).

[81] J. Paulose, Bryan Gin-ge Chen, and V. Vitelli, Topological modes bound to dislocations in mechanical metamaterials, Nat. Phys. **11**, 153 (2015).

[82] S. Imhof, C. Berger, F. Bayer, J. Brehm, L. W. Molenkamp, T. Kiessling, F. Schindler, C. H. Lee, M. Greiter, T. Neupert, and R. Thomale, Topolectrical-circuit realization of topological corner modes, Nat. Phys. **14**, 925 (2018).

[83] M. Serra-Garcia, V. Peri, R. Süsstrunk, O. R. Bilal, T. Larsen, L. G. Villanueva, and S. D. Huber, Observation of a phononic quadrupole topological insulator, Nature (London) **555**, 342 (2018).

[84] C. W. Peterson, W. A. Benalcazar, T. L. Hughes, and G. Bahl, A quantized microwave quadrupole insulator with topologically protected corner states, Nature (London) **555**, 346 (2018).